



Account / Revue

Adhesion at polymer–polymer interfaces: a rigidity percolation approach

Richard P. Wool *

Department of Chemical Engineering, University of Delaware, Newark DE 19716-3110, USA

Received 19 November 2004; accepted after revision 21 March 2005

Available online 11 November 2005

Abstract

A theory of fracture of entangled polymer interfaces was developed which was based on the bridge entanglement concept and the vector percolation model of Kantor and Webman, in which the modulus E is related to the lattice bond fraction p , via $E \sim [p - p_c]^2$. The Hamiltonian for the lattice was replaced by the strain energy density function of the bulk polymer, $U = \sigma^2/2E$, where σ is the applied stress and p was expressed in terms of the normalized entanglement density ν , using the entanglement molecular weight, $\nu \sim M_e^{-1}$. The polymer fractured critically when p approached the percolation threshold p_c , which was accomplished by utilizing the stored strain energy in the network to randomly disentangle or fracture $[p - p_c]$ bonds. The fracture energy was found to be $G_{1c} \sim [p - p_c]$. When applied to interfaces of width X , containing an areal density Σ of chains, each contributing L minor chain entanglements, the percolation term $p \sim \Sigma LX$ and the percolation threshold was related to Σ_c , L_c , or X_c . This gave a unified theory of fracture for the virgin state of polymers in the bulk and a variety of polymer interfaces. The fracture strength σ of amorphous and semicrystalline polymers in the bulk could be well described by the net solution, $\sigma = [E D_o \rho/16 M_e]^{1/2}$, where D_o is the bond energy and ρ is the density [R.P. Wool, J. Polym. Sci., Part A: Polym. Phys. 43 (2005) 168]. It was found to be in excellent agreement with a large body of data. Fracture by disentanglement was found to occur in a finite molecular weight range, $M_c < M < M^*$, where $M^*/M_c \approx 8$, such that the critical draw ratio, $\lambda_c = (M/M_c)^{1/2}$, gave the molecular-weight dependence of fracture as $G_{1c} \sim [(M/M_c)^{1/2} - 1]^2$. The critical entanglement molecular weight is related to the percolation threshold p_c , via $M_c = M_e/(1 - p_c)$ and combined with reptation dynamics, entanglement percolation gave an apparent 3.4 power law for the zero-shear melt viscosity $\eta_o \sim M^{3.4}$. Fracture by bond rupture was in accord with Flory's suggestion, i.e. $G/G^* = [1 - M_c/M]$. For welding of A/A symmetric interfaces, $p = \Sigma LX$, and $p_c \approx L_c/M \approx 0$, such that when $\Sigma/X \sim 1/M$ for randomly distributed chain ends, $p \sim L \sim (t/M)^{1/2}$, $G/G^* = (t/\tau^*)^{1/2}$, where $\tau^* \sim M$, when $M > M^*$, and $\tau \sim M^3$, when $M < M^*$. When the chain ends are segregated to the surface, Σ is constant with time and $G/G^* = [t/\tau^*]^{1/4}$. For sub- T_g welding, there exists a surface mobile layer of depth $X \sim 1/\Delta T^\nu$ such that $G \sim \Delta T^{-2\nu}$. For incompatible A/B interfaces of width d , normalized width w , and entanglement density $N_{ent} \sim d/L_e$, $p \sim d$ such that $G \sim [d - d_c]$, $G \sim [w - 1]$, and $G \sim [N_{ent} - N_c]$. For incompatible A/B interfaces reinforced by an areal density Σ of compatibilizer chains, L and X are constant, $p \sim \Sigma$, $p_c \sim \Sigma_c$, such that $G \sim [\Sigma - \Sigma_c]$. The percolation approach unifies and interrelates the different theories and experiments on a variety of symmetric and asymmetric interfaces by providing a general connectivity relation for structure and strength. The correct time and molecular weight dependence of welding above and below T_g are predicted with a logical extension to the fully healed or virgin strength for linear polymers, rubbers, thermosets and polymer–solid interfaces. **To cite this article:** R.P. Wool, C. R. Chimie 9 (2006). © 2005 Académie des sciences. Published by Elsevier SAS. All rights reserved.

* Corresponding author.

E-mail address: wool@che.udel.edu (R.P. Wool).

Résumé

Une théorie de la rupture d'interfaces polymères enchevêtrées a été développée en se fondant sur le concept de ponts enchevêtrés et sur le modèle du vecteur de percolation de Kantor et Webman, modèle dans lequel le module E est lié à la fraction de liaisons du réseau p par la relation $E \sim [p - p_c]^\tau$. Le hamiltonien pour le réseau est remplacé par la fonction densité d'énergie de déformation du polymère massique $U = \sigma^2/2E$, expression dans laquelle σ est la contrainte appliquée et p est exprimé en termes de densité d'enchevêtrements normalisée ν , en utilisant la masse molaire d'enchevêtrement $\nu \sim M_c^{-1}$. Le polymère subit une fracture critique lorsque p tend vers le seuil de percolation p_c , ce qui correspond à l'énergie de déformation emmagasinée dans le réseau pour désenchevêtrer ou rompre les liaisons $[p - p_c]$ de manière aléatoire. L'énergie de rupture G_{1c} est proportionnelle à $[p - p_c]$. Lorsqu'il est appliqué à des interfaces d'épaisseur X comportant une densité de chaînes Σ par unité de surface, chacune contribuant à des enchevêtrements mineurs L , le terme de percolation s'écrit $p \sim \Sigma L/X$ et le seuil de percolation devient fonction de Σ_c , L_c ou X_c . Cela conduit à une théorie unifiée de la rupture pour les polymères vierges dans leur état massique et pour une grande variété d'interfaces polymères. La résistance à la rupture σ de polymères massiques amorphes et semi-cristallins peut aussi être décrite par l'expression $\sigma = [E D_0 \rho / 16 M_c]^{1/2}$ [R.P. Wool, J. Polym. Sci., Part A: Polym. Phys. 43, 168 (2005)] Un excellent accord a été obtenu pour un grand nombre de résultats. La rupture par désenchevêtrement a été observée pour une gamme de masses molaires $M_c < M < M^*$, avec $M^*/M_c \approx 8$, telles que le rapport critique d'élongation $\lambda_c = (M/M_c)^{1/2}$ conduise à une fonction de l'énergie de rupture avec la masse molaire de la forme $G_{1c} \sim [(M/M_c)^{1/2} - 1]^2$. La masse molaire critique d'enchevêtrement est liée au seuil de percolation p_c par $M_c = M_c/(1 - p_c)$ et, en faisant intervenir la dynamique de reptation, l'enchevêtrement de percolation révèle une viscosité à l'état fondu à cisaillement nul, de type $\eta_0 \sim M^{3.4}$. La rupture par scission des liaisons est en accord avec la suggestion de Flory, à savoir $G/G^* = [1 - M_c/M]$. Dans le cas du soudage d'interfaces symétriques A/A, $p = \Sigma L/X$ et $p \approx L_c/M = 0$, de telle manière que lorsque $\Sigma/X \sim 1/M$ pour des extrémités de chaînes distribuées aléatoirement, $p \sim L \sim (t/M)^{1/2}$, $G/G^* = (t/\tau^*)^{1/2}$, où $\tau^* \sim M$ quand $M > M^*$ et $\tau^* \sim M^3$ quand $M < M^*$. Quand les extrémités de chaînes sont ségréguées vers la surface, Σ est constant avec le temps et $G/G^* = [t/\tau^*]^{1/4}$. Dans le cas de soudages effectués à des températures inférieures à T_g , il se crée une couche superficielle mobile d'épaisseur $X \sim 1/\Delta T^v$, de sorte que $G \sim \Delta T^{2v}$. Pour des interfaces incompatibles A/B d'épaisseur d , d'épaisseur normalisée ω et de densité d'enchevêtrement $N_{ent} \sim d/L_c$, on obtient $p \sim d$, ce qui conduit à $G \sim [d - d_c]$, $G \sim [\omega - 1]$ et $G \sim [N_{ent} - N_c]$. Pour des interfaces incompatibles A/B renforcées par des chaînes de compatibilisant de densité surfacique Σ , L et X sont constants, $p \sim \Sigma$, $p_c \sim \Sigma_c$, de telle manière que $G \sim [\Sigma - \Sigma_c]$. Cette approche sous l'angle de la percolation permet d'unifier et de corrélérer les différentes théories et expériences relatives à une grande variété d'interfaces symétriques et asymétriques, en fournissant une relation générale liant structure et résistance. Les relations entre temps et masse molaire sont prévues correctement dans le cas de soudages en dessous et au dessus de T_g avec l'extension logique à la prévision de la résistance de polymères linéaires, caoutchouc, thermodurcissables et interfaces polymère-solide, à l'état vierge ou parfaitement cicatrisé. **Pour citer cet article** : R.P. Wool, C. R. Chimie 9 (2006).

© 2005 Académie des sciences. Published by Elsevier SAS. All rights reserved.

Keywords: Polymer interface; Fracture; Fatigue; Percolation; Viscosity; Welding; Incompatible; Compatibilizer

Mots-clés : Interface polymère ; Résistance ; Soudage ; Percolation ; Incompatible ; Viscosité ; Fatigue

1. Introduction

In this paper, we explore a new approach to understanding the molecular aspects of adhesion at polymer-polymer interfaces. Percolation theory is used as a means to parameterize the making and breaking of connectivity at polymer-polymer interfaces [1,2]. The strength G_{1c} , of polymer interfaces has been investigated by many [1–52], and different theories have been proposed to relate interface structure to strength. For welding symmetric A/A interfaces as a function of dif-

fusion depth X , it was suggested that $G_{1c} \sim X$ [4–7], or the number of bridges per unit area of interface, P , $G_{1c} \sim P$ [9–14], or the crossing density ρ , $G_{1c} \sim \rho$ [8], or the contour length L , $G_{1c} \sim L$ [16–20]. For incompatible A/B interfaces as a function of equilibrium width w , it has been suggested that $G_{1c} \sim w^2$ [21,22], or $G_{1c} \sim w$ [22]. For incompatible A/B interfaces as a function of the number of entanglements N , in the interface, the relation $G_{1c} \sim N^2$ was proposed [23]. For an incompatible A/B interface reinforced with Σ compatibilizer chains per unit area, $G_{1c} \sim \Sigma^2$, has been sug-

gested [24–31]. Other approaches to analyzing the strength of interfaces have involved simulations [32–34], theoretical modeling [34–41], experimental correlation between toughness and interfacial width [42–49], non-isothermal modeling of composite interfaces [50] and sub- T_g welding [51,52]. Theories relating structure to strength were proposed or utilized for each specific interface, and while all had a measure of success in describing the strength of a targeted interface, essentially none were readily transferable to describe other interfaces, or could be readily extended to provide an acceptable theory of strength for the bulk polymer. Thus, for example, no one has a theory that can simultaneously model strength development during welding of symmetric A/A interfaces and which can be readily extended to understanding the reinforcement of incompatible A/B interfaces by Σ compatibilizer chains, while at the same time predicting the molecular weight dependence of the virgin state. Even within a single interface type, such as welding of symmetric A/A polymer–polymer interfaces, there is little agreement between investigators. The Wool–O’Connor model [16] appears to have the correct form theoretically and experimentally [1] such that the fracture energy G as a function of time t and molecular weight M , behaves as $G \sim L \sim (t/M)^{1/2}$. However, we can criticize the relation $G \sim L$ since it does not have the number of chains per unit area Σ involved. Consequently, if we have just one chain of length L compared to 10^{14} chains, the average L can be the same in both cases

but the strength can be radically different. Thus, we are unable to describe the data of Brown et al. [24–31] for reinforcement of A/B incompatible interfaces with Σ A–B compatibilizer chains, or derive the Brown Law [25], $G \sim \Sigma^2$. Therefore, the early Wool theory of welding cannot be readily extended to other interfaces, even though it appears to correctly predict the molecular weight dependence of the virgin fully healed state [1]. The purpose of this paper is to provide a theory of fracture, which can be applied universally to all interfaces and can be readily extended to understanding the bulk strength of polymers in terms of known microscopic parameters and material constants.

The general approach to evaluating the fracture energy G_{1c} of polymer interfaces is represented in Fig. 1 [1]. Material A is brought into contact with material B to form an A/B interface, the sample is fractured and the strength is related to the structure of the interface through microscopic deformation mechanisms. In the virgin state, or when welding or crack healing, $A = B$. For the incompatible A/B interface, we consider both the non-reinforced interface, and the interface reinforced with an areal density Σ of compatibilizer chains. Typically, a crack propagates through the interface region preceded by a deformation zone at the crack tip. For cohesive failure, the fracture energy can be determined by the J -Integral method, as described by Hutchinson et al. [53–55], where G_{1c} is the integral of the traction stresses $\sigma(\delta)$ with crack opening displacements δ , in the cohesive zone, following yielding at a

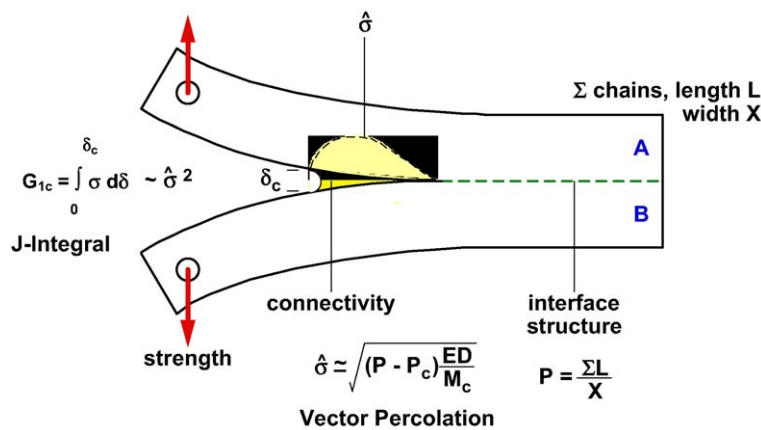


Fig. 1. The microscopic entanglement structure, e.g. at an interface or in the bulk, is related to the measured macroscopic fracture energy G_{1c} via the RP theory of breaking connectivity in the embedded plastic zone (EPZ) at the crack tip. The RP theory determines σ_{max} in the EPZ, which is related to G_{1c} via Hutchinson’s J -Integral theory. The percolation parameter p is related to the interface molecular structure via $p \sim \Sigma L/X$, where Σ is the number of chains of length L in an interface of width X .

local yield or craze stress σ_Y . The cohesive zone at the crack tip breaks down by a vector percolation process, as described herein, at a maximum stress value, $\sigma_m > \sigma_Y$. Typical ratios of σ_m/σ_Y are about 4–10 [53]. Both σ_m and δ are rate dependent and in the simplest case, the fracture energy is determined by:

$$G_{1c} = \sigma_m \delta_m \quad (1.1)$$

where δ_m is the critical crack opening displacement. Both σ_m and δ_m depend on the interface structure and the microscopic deformation mechanisms controlling the percolation fracture process via disentanglement and bond rupture. In this paper, we use the Rigidity Percolation (RP) theory of fracture [3] and apply it to several cases involving (1) fracture of polymer–polymer welds, (2) fracture of incompatible A/B interfaces, and (3), fracture of incompatible interfaces reinforced with Σ compatibilizer chains.

2. Rigidity percolation theory of fracture

The transmission of forces through a lattice as a function of the fraction p , of bonds in the lattice has been analyzed by Kantor and Webman [56], Feng and Sen [57,58], Thorpe et al. [58,59] and others [1,60,61]. De Gennes first suggested that conductivity or scalar percolation could be used to quantize the modulus of elasticity E , of randomly connected networks, such as gels [62]. Analyses based on the Born and Huang model of the microscopic elasticity of a lattice [63] gave results for the elasticity which resembled conductivity percolation when shear terms were neglected in the Hamiltonian for the elastic energy, as:

$$E \sim [p - p_c]^t \quad (2.1)$$

where p is the occupied fraction of lattice bonds, p_c is the percolation threshold and the conductivity exponent, $t \approx 1-2$. However, when shear terms dominated the elasticity, a new form of elasticity began to emerge which potentially belonged to a new universality class than conductivity percolation. Kantor and Webman reformulated the Hamiltonian for the elastic energy, accounting for both tensile bond stretching and angle bending between the fractal, tortuously connected, ‘strings’ of connected bonds remaining in the lattice near p_c , and the macroscopic

elasticity became [56] $E \sim [p - p_c]^\tau$, where τ is the rigidity percolation exponent, which is larger than the conductivity (or scalar) percolation exponent t , in Eq. (2.1). The rigidity percolation threshold p_c can also be greater than the scalar percolation threshold, which is due to the ‘sloppiness’ of the lattice near p_c , thus for example, allowing the transmission of electrons through the weakly connected fractal structure, but not the sensible transmission of vectors.

The vector or rigidity percolation process addresses several important points. First, consider a 2-D lattice near the percolation threshold p_c , as shown in Fig. 2. Due to the random fractal connectivity of the lattice, the stress distribution $\phi(\sigma)$, in the bonds becomes highly non-uniform such that some bonds are highly stressed, while others bear little stress. The existence of highly stressed bonds is a prelude to molecular fracture and parallels the ‘hot bonds’ in conductivity percolation, where hot bonds arise from high current density in some individual bonds near the percolation threshold. The hot bonds overheat like electrical fuses in the high current density and break. The concept of mechanical ‘hot bonds’ is relevant to fracture of polymers in general and is the basis for understanding why materials fracture at macroscopic stresses, which are orders of mag-

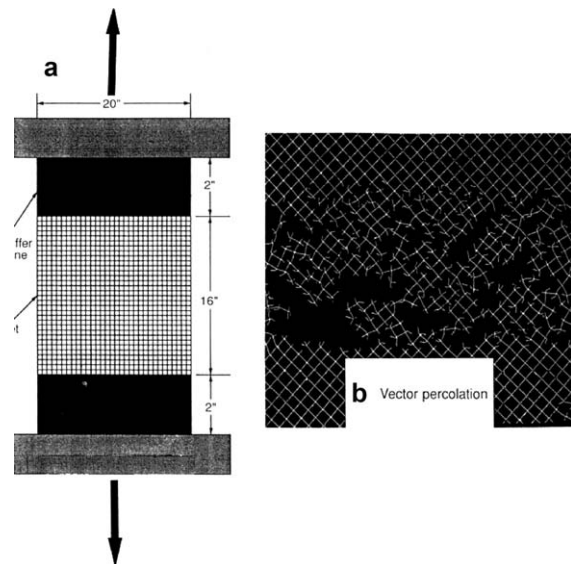


Fig. 2. The role of percolation in the random fracture of bonds in a model net at constant strain is shown [1]. (a) The net, of modulus E , is stressed in uniaxial tension to a stress σ and stores strain energy $U = \sigma^2/2 E$. (b) Release of the stored energy causes random fracture events in the net resulting in a percolating system near the fracture threshold and a very broad distribution of stress on the bonds.

nitude less than the molecular fracture stresses. When polymers such as polypropylene and polyethylene are subjected to uniform tensile stresses, it has been shown using infrared and Raman spectroscopy that the molecular stress distribution can be quite broad, even though the applied stress is well below the macroscopic fracture stress [64,65]. The development of the molecular stress distribution $\phi(\sigma)$ is due to the inherent sloppiness of the lattice. Thus, in the J -integral fracture mechanics model, the maximum fracture stress near the crack tip σ_m , described in Fig. 1 and Eq. (1), remains closer to the yield stress than to the much higher molecular fracture stress.

Another point of interest is that only a fraction $[p - p_c]$ of the bonds needs to be fractured before complete failure occurs in a 2-D or 3-D network. Thus, in a deformation zone at a crack tip, the crack advances through the zone by breaking a fraction $[p - p_c]$ of bonds or fibrils in parts of a craze network. The broken bonds do not lie on the same plane, as is in the Nail Solution [40], and is often assumed intuitively, but are distributed over the deformation zone volume. The deformation zone near fracture is best described as a volume of material preceding the crack tip that contains a considerable number of defects.

An important corollary to the existence of the threshold p_c is that when $p < p_c$, the lattice connectivity is broken and no significant strength exists beyond that of non-bonded potentials and Van der Waals interactions. Thus, the molecular lengths ($L \sim M$) must be long enough, the areal density of chains Σ , at the interface must be great enough and the number of entanglements in the lattice N , at an interdiffusion distance X , or interface width w , has to exceed the percolation threshold before strength develops. This means that an initial investment (p_c) is needed before strength develops, such that when $G_{1c} \sim [p - p_c]$, there exists corresponding critical parameters such as $M_c, L_c, \Sigma_c, X_c, N_c, w_c$, etc., which are all related to each other through the percolation parameter p .

To convert these percolation concepts into quantitative fracture terms, consider the vector percolation experiment shown in Fig. 2, applied to any 3-D lattice in general with tensile modulus E . The Hamiltonian for the stored elastic energy can be formulated using the Born and Huang [63], or the Kantor and Webman approach for specific lattices [56], or using the more simple engineering strain energy density approach as

follows. The stored elastic strain energy density U in the lattice due to an applied stress σ is determined in the uniaxial approximation by:

$$U = \sigma^2 / 2 E \quad (2.2)$$

The stored strain energy can also be determined for the general case of multiaxial stresses [1] and lattices of varying crystal structure and anisotropy. The stored strain energy dissipation per unit volume U_f to fracture a network consisting of a bond (or entanglement) density of ν bonds per unit volume is:

$$U_f = \nu D_o [p - p_c] \quad (2.3)$$

where D_o is the bond fracture energy, and $[p - p_c]$ is the percolation fraction of bonds which must be broken to cause fracture in the network. In this approach, the strain energy U , is first stored in the net and we inquire if this energy is sufficient to break $[p - p_c]\nu$ bonds per unit volume when it releases at a critical strain energy density $U^* = \sigma^{*2} / 2 E$, such that at the critical condition, $U^* \geq U_f$. Substituting for U^* and U_f and solving for the critical stress σ^* , we obtain the 'Net solution' for the critical fracture stress as:

$$\sigma^* = \{2 E \nu D_o [p - p_c]\}^{1/2} \quad (2.4)$$

This equation predicts that the fracture stress increases with the square root of the bond density. The percolation parameter p , is in effect, the normalized bond density such that for a perfect net without defects, $p = 1$, and for a net that is damaged or contains missing bonds, then $p < 1$. Obviously, as p approaches p_c , the fracture stress decreases towards zero and we have a very fragile material. This fracture relation could therefore be used to evaluate durability, or retention strength of a material by tracking damage accumulation through a single parameter p . Note that the Net solution refers to the stress required to fracture a unit volume of the net in uniaxial tension.

When applied to interfaces, we let the volume of material or Net, contain the interface such that we can calculate σ^* with a knowledge of p based on a local normalized entanglement density. In all applications of the RP model, the stressed state is the reference state to assess percolation and connectivity. This will become more apparent when we examine disentanglement for example, where an unraveling or disentanglement process in the stretched state breaks the connectivity.

3. Fracture by disentanglement

The bridge percolation model of entanglements proposed by Wool [1,66] was recently supported by computer simulations of Theodorou et al. [67,68] and is the basis for the disentanglement model described herein. M_c represents a segment of an entangled chain that is long enough to form a bridge or loop of 3-crossings (3P) through a plane in the melt. An entangled net forms when the number of chain ($\Sigma \sim M^{1/2}$) intersecting the plane equals the number of bridges. Thus, when $\Sigma = 3P$, $M_c = 9(\Sigma P)^2 M$. Computer simulations of polyethylene melts by Uhlherr et al. [67] showed this model to be accurate. By sampling the amorphous melt, they found that the average mesh segment which intersected the plane three times was equivalent to the critical entanglement molecular weight M_c . Thus, the bridge with three crossings is the basic mesh element of the entanglement network capable of transmitting vectors and defines precisely the number of bonds per chain which must be broken or disentangled to obtain a critically connected structure.

Disentanglement is considered to proceed by the mechanism shown in Fig. 3, where we depict the response of an (average) entangled chain to a constant (step function) draw ratio λ [1,3]. Fracture by disentanglement occurs by first straining the chains to a critical draw ratio λ_c and storing mechanical energy of order

$G \sim (\lambda_c - 1)^2$. The stretched chains then relax by Rouse-like retraction and disentangle, when the energy released is sufficient to relax them to the critically connected state corresponding to the percolation threshold, p_c . When this occurs, a chain, which initially had many bridges ($\sim M^{1/2}$), is reduced to a single critically connected bridge by the applied strain. The percolation parameters [$p - p_c$] associated with the disentanglement process at an interface are derived as follows; p is the normalized entanglement density defined as:

$$p = g(\lambda) N_v / v \quad (3.1)$$

where $g(\lambda)$ is the number of entanglements per chain, N_v is the number of chains per unit volume and v is the entanglement density of the perfect net. We define $g(\lambda)$ as:

$$g(\lambda) = [M/M_c(\lambda)] - 1 \quad (3.2)$$

The chain ends effectively contribute to the loss of one entanglement. Since $N_v = \rho/M$ and $v = \rho/M_c$, then we have:

$$p = \frac{\{[M/M_c(\lambda)] - 1\} \rho/M}{\rho/M_c(\lambda)} \quad (3.3)$$

such that:

$$p = [1 - M_c(\lambda)/M] \quad (3.4)$$

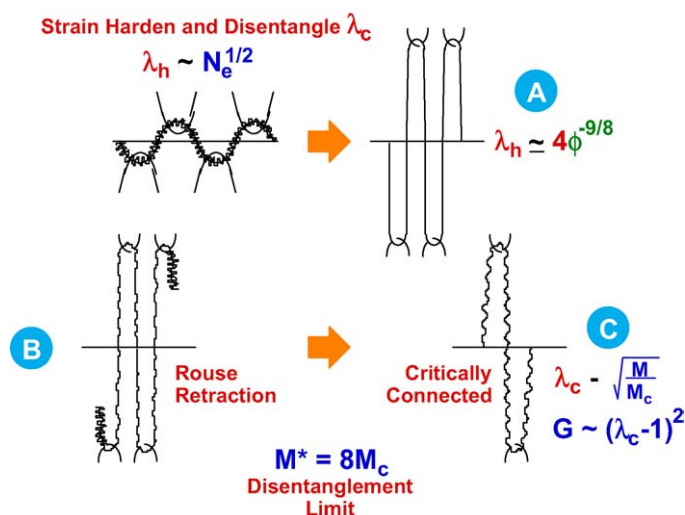


Fig. 3. Disentanglement mechanism. (A) Tightened slack between entanglements. (B) Retraction and disentanglement by Rouse relaxation. (C) Critically connected entangled state at draw ratio λ_c , where the chain has been reduced to a bridge with 3 crossings of the interface plane.

where $M_e(\lambda)$ is the stretch-dependent M_e value after it has relaxed to position C, as shown in Fig. 3. $M_e(\lambda)$ is given by the following approximation:

$$M_e(\lambda) = \lambda^2 M_e \quad (3.5)$$

$M_e(\lambda)$ increases between entanglement points due to the retraction process at constant λ . A more detailed treatment of disentanglement would account for the orientation function of the entanglements and lateral contraction, as discussed elsewhere [1]. Eq. (3.4) becomes:

$$p = 1 - \lambda^2 M_e/M \quad (3.6)$$

An important consequence of the latter equation is that when $\lambda = 1$, there exists a critical value of molecular weight $M = M_c$ for which $p = p_c$ and we obtain the relation between M_e and M_c as:

$$M_c = \frac{M_e}{1 - p_c} \quad (3.7)$$

Since $p_c \approx 1/2$, we note that $M_c \approx 2 M_e$, as commonly observed. M_e is determined from the onset of the rubbery plateau by dynamic mechanical spectroscopy and M_c is determined at the onset of the highly entangled zero-shear viscosity law, $\eta \sim M^{3.4}$. This provides a new interpretation of the critical entanglement molecular weight M_c , as the molecular weight at which entanglement percolation occurs with the onset of long-range connectivity. Concomitantly, the dynamics changes from single chain, Rouse-like behavior, to that of chains significantly impeded by others, as in Reptation. It also represents the transition from the Nail (weak fracture) to the Net (strong fracture) solution and the onset of significant strength development via the formation of stable, strong, oriented fibrillar material in the deformation zones preceding the crack advance.

When $M > M_c$, we obtain the critical draw ratio for fracture λ_c from Eq. (3.6) as:

$$\lambda_c \approx (M/M_c)^{1/2} \quad (3.8)$$

The maximum molecular weight M^* at which disentanglement can occur is determined when strain hardening occurs at $\lambda_c \approx 4$ such that¹:

$$M^* \approx 8 M_c \quad (3.9)$$

Donald and Kramer [69] also found that the draw ratio of crazes in several polymers was of order $\lambda \approx 4$ and varied in a range of 2–5. In 1981, A. Donald explained to R.P. Wool (private communication) the significance of straightening the slack between entanglements, which is key to understanding the disentanglement process described herein. At $M = M^* = 8 M_c$, $G^* \sim 0.42 M^*$ such that Eq. (3.8) gives the molecular weight dependence of the virgin-state fracture energy as [1]:

$$G_{1c}/G^* = 0.3 M/M_c [1 - (M_e/M)^{1/2}]^2 \quad (3.10)$$

We have shown that the latter equation gives an excellent fit to the molecular weight dependence of fracture [3]. At high rates of strain compared to $1/\tau$, the inverse disentanglement time, or when disentanglement cannot readily occur ($M > M^*$), bond rupture occurs randomly in the network and the percolation parameter p becomes dominated by chain ends. In this case, the entanglement molecular weight M_e does not depend on strain and Eq. (3.4) gives:

$$p = 1 - M_e/M \quad (3.11)$$

Since $G_{1c} \sim [p - p_c]$, and $p_c = 1 - M_e/M_c$, we obtain:

$$G_{1c} = G^* [1 - M_e/M] \quad (3.12)$$

where G^* is the plateau fracture energy at high molecular weight. The latter equation is identical to the empirical relation for the molecular weight dependence of fracture suggested by P.J. Flory, who coincidentally developed the first percolation theory applied to polymer gelation [70].

In addition to glassy polymers, the RP-fracture model also describes the fracture of soft lightly crosslinked rubber materials, as described in detail elsewhere [3]. Rubber is an interesting case since the modulus E and crosslink density ν in Eq. (2.4) are related via $E \sim \nu$, such that the fracture stress $\sigma \sim E$, $\sigma \sim \nu$ and the fracture energy at low deformation rates behaves as $G_{1c} \sim \nu$. It is also found that a perfect rubber network ($p = 1$) cannot break without first undergoing significant strain hardening at $\lambda \approx 4$, which is the common experience [3].

3.1. Comment on percolation and polymer rheology

Entanglement percolation effects will have a significant effect on the manifestation of rheological func-

¹ The factor of 8 rather than 16 occurs due to an orientation correction [1].

tions associated with the dynamics of disentanglement via Reptation processes, such as the zero shear viscosity η_0 and creep compliance J_e^0 . For example, the zero shear viscosity is well approximated by:

$$\eta_0 = G_N^0 \tau \quad (3.13)$$

where G_N^0 is the plateau modulus and τ is the terminal relaxation time. From de Gennes' reptation theory, $\tau \sim M^3$, such that Eq (3.13) predicts that $\eta_0 \sim M^3$. However, the exponent of 3.0 disagrees with the well-known experimental exponent of 3.4. Many have addressed this problem and no solution is universally accepted. During relaxation, the rigidity percolation process allows the stored elastic energy to relax faster in the terminal relaxation zone. In the melt, the fraction of entanglements $p(t)$, remaining in the entanglement lattice will be well approximated at $t < T_r$ by [1]:

$$p(t) = 1 - 4/\pi^{3/2} [t/T_r]^{1/2} - M_e/M \quad (3.14)$$

where M_e/M is the chain-end correction. From Eq 2.1, the stress relaxation modulus in the terminal zone near percolation is $E(t) = G_N^0[p(t)-p_c]^2$, it follows from Eq. (3.7) and Eq. (3.14) that the critical relaxation time τ_{RP} is determined as:

$$\tau_{RP}/T_r = 1.94 [M_e/M_c - M_e/M]^2 \quad (3.15)$$

When $M = M_c$, $\tau_{RP} = 0$ as expected, and when $M = \infty$, $\tau_{RP} \sim T_r$. Thus, for typical experimental M values in the order of 5–10 M_c , the mechanical relaxation time τ_{RP} is less than the dynamics relaxation time T_r due to rigidity percolation of the entanglement network in the terminal zone. A fraction $[1 - p_c]$ of the entanglements relaxes by the single chain Reptation process and a fraction p_c relaxes by a multichain intermolecular percolation process with a Rouse-like character. This produces an apparent $\eta_0 \sim M^{3.4}$ law and the exponent of 3.4 is a consequence of the percolation process and has no particular scaling law relevance. In the absence of percolation in the terminal zone, since the dynamics relaxation time $\tau \sim R^2/D$, one can also obtain a 3.4 power by requiring that the diffusion coefficient $D \sim M^{-2.4}$ while the end-to-end vector behaves as $R^2 \sim M$. An analysis of diffusion data by Lodge et al. [71] suggested that $D \sim M^{-2.3}$. However, this will not produce mechanical relaxation times that are significantly less than the chain dynamics relaxation time as observed experimentally.

The creep compliance J_e^0 as a function of molecular weight is predicted by the Doi–Edwards theory [72] to be independent of molecular weight for $M > M_c$. However, it is found experimentally that $J_e^0 \sim M$ at values of $M < M^*$ and $J_e^0 \sim M^0$ when $M > M^*$, where $M^* \approx 5$ –8 times M_c . In addition to the 3.4 power for η_0 , it can be readily shown² that the percolation correction also predicts the correct creep behavior using the rheological functions:

$$\eta_0 = G_N^0 \int_0^\infty p(t) dt \quad (3.16)$$

$$J_e^0 = \int_0^\infty t p(t) dt / G_N^0 \left[\int_0^\infty p(t) dt \right]^2 \quad (3.17)$$

Entanglement percolation effects had not previously been considered by any investigator in addressing the above long-standing unresolved issues in polymer rheology.

4. Polymer–polymer welding

Fig. 4 shows an interface formed by random walk chains diffusing by reptation across a polymer–polymer weld line [34]. The molecular aspects of interdiffusion of linear entangled polymers ($M > M_c$) during welding of polymer interfaces are summarized in Table 1 [1]. The Reptation dynamics and the interface structure relations in Table 1 have been demonstrated experimentally by a series of interdiffusion experiments with selectively deuterated polymer–polymer interfaces using Dynamic Secondary Ion Mass Spectroscopy (DSIMS) and Neutron Reflectivity [73–78]. These experiments involved interfaces consisting of the following polymer pairs; HDH/DHD, HDH/HPS, HDH/DPS, DHD/DPS, DHD/HPS and DPS/HPS, where HDH, DHD, DPS and HPS were centrally deuterated (25%) PS chains, End deuterated (25% each end) PS chains, fully deuterated and fully protonated (normal) polystyrene chains, respectively. The HDH/DHD ‘ripple’ experiments clearly showed that DeGennes' reptation dynamics model was an excellent model to describe the interdiffusion process dur-

² R.P. Wool, American Physical Society Meeting (2000).

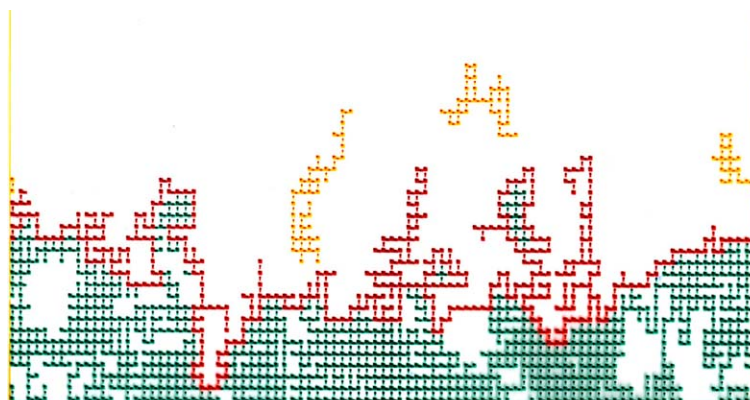


Fig. 4. Polymer interface (one side) formed by random walk chains interdiffusing across the weld line at the bottom. The green chains are the connected chains that contribute to weld strength by connecting both sides of the interface; the yellow chains are those chains that have interdiffused but do not contribute to strength since they are not connected to both sides. The red line is the fractal diffusion front, which divides the connected from the non-connected chains in the diffusion gradient.

ing welding, the HDH/DPS and DHD/HPS showed the distinct motion of the chain ends and centers and the HPS/DPS demonstrated the overall concentration profiles. The scaling laws and the complete concentration profiles were calculated by Kim et al. [19] and Zhang et al. [20]. The important result for the contour length $L \sim (t/M)^{1/2}$, (which is the basis for the early Wool theory) was also supported by welding computer simulations of Windle et al. [32] Initially, as the symmetric ($A=B$) interface wets by local Rouse segmental dynamics, we find that rapid interdiffusion occurs to distances of the order of the radius of gyration of the entanglement molecular weight, ca 3 nm. This can also occur below T_g when the top surface layer becomes more mobile than the bulk and can be explained by finite size rigidity percolation theory [79]. However, at this point, the interface is very weak and fracture can be described by the Nail solution [40]. At the wetting stage,

the frictional pullout of intermeshed chain segments, which have ‘elbowed’ their way across the interface, determines the fracture energy (ca 1 J/m²). As welding proceeds, Σ minor chains of length L diffuse into an interface of width X and considerable strength develops. The diffusing chains are fractal random walks and interpenetrate with chains, which are fully entangled (ignoring surface reflection configuration effects on entanglement density).

The structure of the diffuse weld interface in Fig. 4 resembles a box of width X , with fractal edges containing a gradient of interdiffused chains, as shown by Wool and Long [34]. Using Sapoval’s gradient percolation theory [80], we require that chains, which contribute to the interface strength, straddle the interface plane during welding, such that chains in the concentration gradient which have diffused further than their radius of gyration cease to be involved in the load bearing pro-

Table 1
Molecular aspects of interdiffusion at a polymer–polymer interface

| Molecular Aspect | Symbol | Dynamic relation, $t < T_r$ | Static relation H $t = T_r$ | r, s |
|-----------------------------------|-------------|--------------------------------|--------------------------------|--------|
| General property | $H(t)$ | $t^{r/4} M^{-s/4}$ | $M^{(3r-s)/4}$ | r, s |
| Average contour length | $l(t)$ | $t^{1/2} M^{-1/2}$ | M | 2,2 |
| Number of chains | $\Sigma(t)$ | $t^{1/4} M^{-5/4}$ | $M^{-1/2}$ | 1,5 |
| Number of bridges | $P(t)$ | $t^{1/2} M^{-3/2}$ | M^0 | 2,6 |
| Average monomer diffusion depth | $X(t)$ | $t^{1/4} M^{-1/4}$ | $M^{1/2}$ | 1,1 |
| Total number of monomers diffused | $N(t)$ | $t^{3/4} M^{-7/4}$ | $M^{1/2}$ | 3,7 |
| Center of mass | X_{cm} | $t^{1/2} M^{-1}$ | $M^{1/2}$ | 2,4 |
| Diffusion | | | | |
| Fractal diffusion | N_f | $t^{1/2} M^{-3/2}$ | M^0 | 2,6 |
| Front length | | | | |

cess at the interface. We have shown that this amounts to a very small number and for narrow molecular weight distributions, can be ignored [1,19,20]. However, for broad molecular weight distributions, the fraction of non-connected chains expressed through gradient percolation, can be significant and impacts on the observed time dependence of welding [1 (p. 76)].

When the local stress exceeds the yield stress, the deformation zone forms and the oriented craze fibrils consist of mixtures of fully entangled matrix chains and partially interpenetrated minor chains. Fracture of the weld occurs by disentanglement of the minor chains, or by bond rupture. It is interesting to note that if the stress rises to the point where random bond rupture in the network begins to dominate the deformation mechanism, instead of disentanglement, then the weld will appear to be fully healed, regardless of the extent of interdiffusion. This can occur at high rates of testing when the minor chains cannot disentangle and bond rupture pervades the interface, breaking both the minor chains and the matrix chains.

The percolation term $[p - p_c]$ determines the number of bonds to be broken, or disentangled such that when Σ chains, each with L/L_c entanglements per chain, interdiffuse in an interface of width X , we obtain

$$[p - p_c \sim \{\Sigma L/X - [\Sigma L/X]_c\}] \quad (4.1)$$

where $p_c \sim [\Sigma L/X]_c$. Since $\Sigma/X \sim 1/M$ (Table 1), it follows that $p_c \sim L_c/M$. Thus, when the interdiffused minor chain length $L \approx M_c$, we have no strength (above that of the Nail solution), and when $M \gg M_c$, $p_c \approx 0$, which we will assume henceforth for the welding analysis. In terms of a time argument, the time at which p_c is reached is controlled largely by Rouse segmental dynamics, which is much shorter than the long interdiffusion time determined by reptation dynamics [81,82]. Thus, the slower interdiffusion process will dominate strength evolution vs. time.

The interface of width X is composed of a fraction L/M of diffusing chains and the matrix chain fraction $(1 - L/M)$, into which the chains are diffusing. The total stored strain energy in the interface $U \sim X$, is consumed in disentangling only the Σ minor chains of length L , from the matrix chains, which are being stretched also but cannot disentangle at the same rate as the minor chains, and we obtain, $G_{1c} \sim p$ as:

$$G_{1c} \sim \Sigma L/X \quad (4.2)$$

When the matrix chains disentangle or break along with the interdiffused chains, then $p = 1$ and the virgin strength is reached. The number of diffusing chains per unit area Σ , contributing to the interface strength is governed by gradient percolation, such that only those chains which straddle the interface are counted. Thus, only a subset of the concentration depth profile is contributing to strength, namely, those chains which are simultaneously connected to the A and B side of the interface. Also, the length L implies the number of entanglements per minor chain $(L/L_c - 1)$, which can decrease significantly, for example, if brush-like ordering occurs at the interface, or the entanglement topology changes such that L_c becomes very large as in a solvent where M_c depends on polymer concentration ϕ , as $M_c = M_c(1)/\phi$.

Applying Eq. (3.1), $p = g(\lambda) N_v/v$ to the interface, we obtain the number of entanglements per contour chain length L as, $g(\lambda) = (L/L_c - 1)$, the number of chains in the interface $N_v = \Sigma/X \sim 1/L_\infty$ (from Table 1), the crosslink density $v \sim 1/L_e$, the stretch-dependent entanglement length $L_e(\lambda) = \lambda^2 L_c$, such that Eq. (3.1) gives the percolation parameter:

$$p = (L - \lambda^2 L_c)/L_\infty \quad (4.3)$$

and the percolation threshold p_c is determined at $\lambda = 1$ and critical length $L = L_c$ as:

$$p_c = (L_c - L_e)/L_\infty \approx L_e/L_\infty \quad (4.4)$$

in which $L_c \sim M_c$, $L_e \sim M_e$, $L_\infty \sim M$ and $L_c \approx 2 L_e$. Substituting for $p_c = p$ in Eq. (4.3) and solving for the critical disentanglement length λ_c , we obtain:

$$\lambda_c = [L/L_c - 1]^{1/2} \quad (4.5)$$

Note that when $L = 2 L_e = L_c$, then $\lambda_c = 1$ as required. Also, when strain hardening occurs at $\lambda_c = 4$, then $L^* \approx 8 L_c$, which is the transition from disentanglement to bond rupture as the maximum strength is obtained. Since $G_{1c} \sim (\lambda_c - 1)^2$, and the time evolution of the minor chain length $L \sim (t/M)^{1/2}$ is orders of magnitude longer than that for the entanglement length L_e , the time dependence of welding is given by $G_{1c} \sim L$, as:

$$G_{1c}/G_{1c}^* = [t/\tau^*]^{1/2} \quad (t \leq \tau^*) \quad (4.6)$$

Here G_{1c}^* is the maximum strength obtained at the welding time $\tau^* \sim M$. Note that when $M < M^*$, $L = L_\infty (t/T_1)^{1/2}$ such that $G_{1c} \sim [t/M]^{1/2}$ and full inter-

diffusion of the contour length is required to $L = L_\infty$ and the welding time occurs at $t = T_r$. However, when $M > M^*$, full interdiffusion is not required and full strength is achieved at $L = L^* = 8 L_c$ and $L = L^* (t/\tau^*)^{1/2}$, where $\tau^* \sim M$. For all molecular-weights, the molecular-weight dependence of welding remains as $G_{1c} \sim (t/M)^{1/2}$. Experimental support for Eq. (4.64) was reported by O'Connor [16,17] and McGarel et al. [18] and reviewed in reference [1]. The applicability of the welding law $G_{1c} \sim [t/M]^{1/2}$ has been demonstrated not only for glassy polymers but also for hot-tack experiments and rubbery polymers [1 (Chapter 8)].

Thus, for all welds, there exists a critical interdiffusion distance X^* to obtain the maximum strength G_{1c}^* as:

$$X^* = 0.8 R_g^* \quad (4.7)$$

where R_g^* is the radius of gyration of a polymer with molecular weight $M^* = 8 M_c$. The time to achieve complete strength is related to the reptation time by:

$$\tau^* = 64 (M_c/M)^2 T_r \quad (4.8)$$

such that when $M = 8 M_c$, $\tau^* = T_r$. Quantitative examples for optimal weld designs are given in the next section.

4.1. Fracture vs. fatigue

The full interpenetration of chains (X approaches R_g) is not necessary to achieve complete strength, when $M > M^*$ and $\tau^* < T_r$. However, a cautionary note: while complete strength may be obtained in terms of critical fracture measures, such as G_{1c} and K_{1c} , the durability, measured in sub-critical fracture terms, such as the fatigue crack propagation rate da/dN , may be very far from its fully healed state at τ^* . We have shown that while the weld toughness K_{1c} increases linearly with interdiffusion depth X as $K_{1c} \sim X$, the fatigue crack propagation behavior of partially healed welds behaves as [1,18]

$$da/dN \sim X^{-5} \quad (4.9)$$

This fatigue behavior is a very strong function of interdiffusion depth and underscores the penalty to pay for partial welding. Thus, the weld strength may be deceptively close to the virgin strength, but the fatigue strength may be dramatically reduced below its maxi-

imum value. Thus, one should always design a welding temperature-time process window with respect to T_r to achieve maximum durability of welds and interfaces.

The welding times can be readily calculated. The reptation time T_r is determined from the self-diffusion coefficient D and the end-to-end vector R , by [81]:

$$T_r = R^2 / (3 \pi^2 D) \quad (4.10)$$

For example, when welding polystyrene at 125 °C, $D = 4 \times 10^{-6} / M^2$ (cm²/s) [77,84], $R^2 = 0.45 \times 10^{-16} M$ (cm²) such that $T_r = 4 \times 10^{-13} M^3$ (s) and $\tau^* = 0.0234 M$ (s). For the case where $M = 400\,000$ g/mol and $M_c = 30\,000$ g/mol, we have $\tau^*/T_r = 0.36$, where $T_r = 435$ min and $\tau^* = 156$ min. In this example, if the maximum weld strength were obtained at an allowed welding time of 156 min, the durability as measured by da/dN , would only be about 1/5 of its virgin value compared to complete welding at $T_r = 435$ min. When plastic parts are being injection molded, laminated, sintered or co-extruded, many internal weld lines are encountered and this aspect of welding needs to be considered in designing materials with optimal durability [1].

Recent studies [83] have suggested that while chains diffuse in a reptation-like mode, the monomer friction coefficient (assumed constant for reptation) may have a weak molecular weight dependence, in the order of $M^{0.3}$, resulting in an exponent of 3.3, instead of 3.0 for the molecular weight dependence of the relaxation time. If true, this would cause a small change in the exponents for the molecular weight dependence of welding, but would not affect the time exponents. For example, the minor chain length L , which from Table 1 behaves as $L \sim t^{1/2} M^{-0.5}$ with $\tau \sim M^3$, would become $L \sim t^{1/2} M^{-0.65}$, when $\tau \sim M^{3.3}$.

4.2. Chain-end segregation

In the case of chain-end segregation to the surfaces, as can occur in crack healing and some latex particle coalescence during film formation, the number of chains Σ is constant and the percolation term becomes $p \sim L/X$, or $p \sim X$, since $X \sim L^{1/2}$. Thus, from Table 1, the strength development would be $G_{1c} \sim (t/M)^{1/4}$, rather than the usual $t^{1/2}$ dependence. This $t^{1/4}$ result was also predicted by Prager and Tirrell, using a crossing density analysis [8], but with a different molecular weight dependence for both the welding and virgin state.

4.3. Welding below T_g

Welding below T_g , as recently demonstrated by Boiko et al. [51,52] can occur due to softening of the surface layer. We have treated the surface layer softening as a gradient rigidity percolation issue [79]. The surface melting and glass transition temperature of thin films is an important issue for nano-materials, thin film coating processes, sealing and welding of polymer materials. A significant number of papers have been published in this field dealing with the dynamics of heterogeneous media near T_g , confinement effects, surface effects, measurement methodology, thin film melting, thermal and mechanical properties. We have treated this thin film and surface mobile layer problem as a finite size vector percolation problem. The percolation threshold is reduced by the thickness of the film due to finite size clusters spanning the film.

The intermolecular bonding between atoms is anharmonic and an atom no longer transmits rigidity when it has thermally expanded beyond a critical distance, ca 0.22 bond strain, which is related to the position of the first derivative (force) maximum in the intermolecular potential energy function. Lindemann, ca 1910, proposed this as a mechanism for melting due to the onset of vibrational instability in the lattice with a sufficient number of LA atoms. This concept was later expanded upon by Born (1939) as the *Shear Rigidity Catastrophe* theory. We have elaborated further on the Born criterion using finite size vector percolation theory. During thermal expansion, we assume that the number of LA is proportional to temperature, and is in dynamic equilibrium such that their fraction $p \sim T$, and $p_c \sim T_g^\infty$, where the latter is the T_g of the bulk glass at infinite thickness. Since the elastic modulus $E \sim [p - p_c]^\nu$, where the exponent $\nu \approx 1$, the glass to rubber transition occurs

when there are sufficient connected clusters of LA atoms at p_c and the high glass modulus decreases towards zero: E does not actually go to zero experimentally since the rubbery modulus is finite.

For thin polymer films containing a fraction p of LA atoms at $p < p_c$, clusters of LA can be accessed and connected from the surface, as shown in Fig. 5. These fractal clusters are dynamic and if the LA were lights turning on and off as bonds are broken and reformed, the clusters would be blinking and dancing with interesting frequencies. We have shown that the accessed fraction f (dark clusters in Fig. 5), can be described by the finite lattice size percolation relation [1],

$$f = S(b/h) [1 - p/p_c]^{-\alpha} (p < p_c) \quad (4.11)$$

where b is the particle diameter, h is the film thickness, S is the number of free surfaces ($S = 3, 2, 1$, or 0) and α is determined by:

$$\alpha = \nu (D - d + 1) \quad (4.12)$$

in which D is the fractal dimension of the clusters, d is the dimension of the sample (typically $d = 2$ for simulations (Fig. 5) and $d = 3$ for films and surfaces) and ν is the cluster correlation exponent, which gives the average size of the cluster as

$$\xi = b |p - p_c|^{-\nu} \quad (4.13)$$

In 3-D, $\nu = 0.8$, $D \approx 2.5$, and $\alpha \approx 0.4$; in 2-D, $\nu = 4/3$, $D \sim 7/4$ and $\alpha \approx 1$. The S -factor in Eq. (4.11) refers to the number of free surfaces of the thin material and this becomes unity if only one surface is free or the film is adhered to a substrate. In Fig. 5, the surface fraction accessed at $p < p_c$ is determined using $d = 2$, $p = 0.58$, $p_c = 0.5927$, $b = 1$, $h = 512$ (lattice size), $D = 7/4$, and $\alpha = 1$, such that Eq. (4.11) predicts that $f \approx 18\%$,



Fig. 5. Finite clusters of Lindemann atoms (LA) (in black) are shown in a thin film of thickness h at $T < T_g$. The LA fraction $p = 0.58$. The surface accessed (dark) connected fraction $f = 17\%$. [1].

which is in close agreement with the computer simulations (17%) at $p < p_c$. The cluster size correlation length in this case was $\xi = 79$ and complete connectivity would occur ($f = 100\%$) if the thickness h were reduced from 512 to 93 lattice units.

When heat is applied to the thin film, as implied in Fig. 5, the free surfaces effectively have a monolayer of liquid atoms, which enhance the connectivity of the LA clusters at the surface. Thermal energy invades from the surface as vibrational waves with random amplitude causing intermolecular dissociation events on the amorphous ‘lattice’ of anharmonically bonded atoms on the polymer chains. Using Equation (4.11), and substituting for $p/p_c = T/T_g^\infty$, the finite size percolation threshold $f(h) = p^*$, such that we obtain the thickness dependence of $T_g(h)$ as:

$$T_g(h) = T_g^\infty [1 - (B/h)^\gamma] \quad (4.14)$$

in which B and γ are described by:

$$B = S b / p^* \quad (4.15)$$

$$\gamma = 1/[v(D-d+1)] \quad (4.16)$$

The parameter S can have values of 0, 1, 2, or 3. For two free surfaces, $S = 2$, and the value of $B \approx 0.8$ is determined using $b = 0.154$ nm for a C–C bond, and a percolation threshold $p^* = 0.4$. For one free surface, e.g., a bulk surface or a thin film deposited on a neutral substrate, $S = 1$, and $B = 0.4$; for a thin film in contact with two neutral surfaces, $S = 0$ and $B = 0$, such that the thin film properties are the same as the bulk; for $S = 3$, e.g., with 3-D nano-particles of volume $V \sim h^3$, then $B \approx 1.16$, which shows the greatest effect of T_g reduction with h . For strongly adsorbing thin films, the mobility of the surface layer is suppressed and T_g and T_m will actually increase relative to the bulk value. Thin films with one side free and the other side strongly adsorbed could provide some interesting local mobility battles. The value of γ is determined by the vector percolation values of v and D , and is of order unity. For example with $d = 3$, $v = 0.82$ and $D = 2.85$, Eq. (4.16) gives $\gamma = 1.44$. This relation for $T_g(h)$ is in accord with data recently obtained by several investigators [85,86].

The surface rubbery layer concept-controversy in thick films is interesting and this percolation theory suggests that for free welding surfaces with $S = 1$, it exists, but there is a gradient of $p(x)$ near the surface, where

$x < \xi$ as implied in Fig. 5, and hence a gradient in both T_g and modulus E . If the gradient of p is given by $p(x) = (1 - x/\xi)$, then the value of X_c for which the gradient percolation threshold p_c occurs, and which defines the thickness of the surface mobile layer, is given by the percolation theory as:

$$X_c = b(1 - p_c) / \{p_v^c [1 - T/T_g] v\} \quad (4.17)$$

such that $X_c \sim 1/\Delta T^v$. For example, if $T = (T_g - 10)$, $b = 0.154$ nm, $p_c = 0.4$, $v = 0.82$, then the thickness of the mobile layer $X^* = 3.8$ nm. This could allow for healing to occur below T_g assuming that the dynamics are fast enough, since the mobile layers on both surfaces effectively disappear when the interface is formed. If $G_{1c} \sim X^2$ for entangled polymers, then we could deduce from Eq. (4.17) that for sub- T_g healing at $\Delta T = T_g - T$:

$$G_{1c} \sim \Delta T^{-2v} \quad (4.18)$$

This appears to be in qualitative agreement with Boiko’s data [52], who examined the fracture energy of polystyrene interfaces during welding at temperatures up to 80°K below T_g .

4.4. Summary comment on welding

In summary, the strength development during welding of polymers is well described by the relation:

$$G_{1c} = G_{1c}^* (t/\tau)^{1/2} \quad (4.19)$$

where G_{1c}^* is the virgin strength determined by the percolation theory (Eq. (3.10)), and τ is the welding time, such that $\tau \sim M$ when $M > M^*$, and $\tau \sim M^3$ when $M < M^*$. Equation (4.19) reflects the scaling law for welding processes which are dominated by the diffusion stage of healing. However, as discussed in detail elsewhere [1,16], the other stages of welding, such as surface approach, surface rearrangement, wetting and randomization can play a major role in the time dependence of the overall strength development. It is also important to note that G_{1c} is not a simple function of interdiffusion depth X , for all depths, since the transition from the nail (weak-simple pullout) to the net (strong-entangled) solution occurs at a particular value of X_c , of order R_{ge} . This transition will be important in incompatible amorphous interfaces, as discussed in the next section.

5. Fracture of incompatible interfaces

Consider the incompatible A/B polymer interface shown in Fig. 6. The equilibrium interface width d , which is typically much less than R_g of either the A or B chains, can be described by the Helfand relation [35]:

$$d = 2b/(6\chi)^{1/2} \quad (5.1)$$

in which χ is the Flory–Huggins interaction parameter and b is the random-walk bond length. The interface thickness d , derives from a minimum in the free energy of mixing F , associated with the positive relief of entropy S , of surface confined chain segments of length L ($S \sim k \ln L$) as they blossom forth across the interface, counterbalanced by the negative enthalpy of mixing H , of incompatible A–B segments ($H \sim \chi L$). Letting the free energy $F = H - TS$ and evaluating the free-energy minimum, $dF/dL = 0$, the equilibrium mixing length is obtained as:

$$L \sim kT/\chi \quad (5.2)$$

Since the interface width $d \sim L^{1/2}$, the equilibrium incompatible interface thickness is derived as $d \sim 1/\chi^{1/2}$, as expressed by Helfand in Eq 5.1. With increasing compatibility, or as χ approaches zero, d approaches the normal interface width $X \sim R_g$ and the intermeshing segments becomes highly entangled, thereby producing much higher fracture energy comparable to the virgin state [1,21].

To understand the strength G , of incompatible interfaces as a function of their width d , we first consider the random walk of length L , shown in Fig. 6. This length L is part of a much larger random walk chain, and is a segment which begins on the B-side and

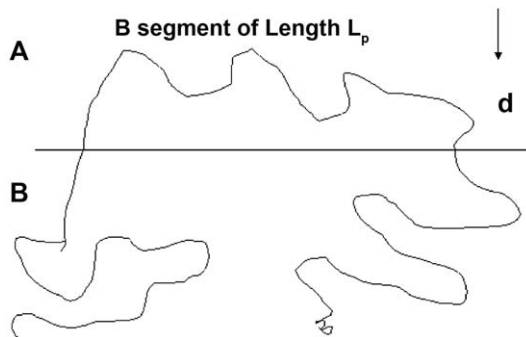


Fig. 6. Shows a chain segment of length L_p of a B-chain as it forms a bridge across an A/B incompatible interface of width $d \sim L_p^{1/2}$.

traverses into the A-side, and returns to the B-side. In this respect, it is a bridge segment (of a larger chain) of length L_p , rather than a free chain of length L , such that the equilibrium interface width is properly described by:

$$d \sim L^{1/2} \sim L_p \quad (5.3)$$

The number of bridges per unit area crossing the A/B interface is Σ_p , which is independent of molecular weight. As L_p increases, entanglements develop, crazes form and the percolation relation $G \sim [p - p_c]$ applies. Here, the percolation parameter $p = \Sigma L/X$ is now defined by:

$$p \sim \Sigma_p(L_p/L_c)/d \quad (5.4)$$

where L_p/L_c is the number of entanglements per bridge. Since $d \sim L_p^{1/2}$, we obtain $p \sim d$, $p_c \sim d_c$, and hence:

$$G \sim [d - d_c] \quad (5.5)$$

Here d_c is the critical interface width corresponding to p_c , which will be in the order of R_{ge} , and below which no strength exists, other than that of simple pullout and surface energy terms, as described by the nail solution. Letting the normalized width $w = d/d_c$, Eq. (5.5) becomes:

$$G \sim [w - 1] \quad (5.6)$$

The maximum strength G^* is determined by:

$$G^* \sim [w^* - 1] \quad (5.7)$$

where $w^* \approx (M^*/M_c)^{1/4} \approx 2$. Thus, the ratio G/G^* becomes:

$$G/G^* = (w - 1)/(w^* - 1) \quad (5.8)$$

To investigate the latter relation, a plot of G/G^* vs. w , should have a slope of $1/(w^* - 1) \approx 1$, an intercept on the w axis at $w_c = 1$, and maximum strength attained ($G/G^* = 1$) at $w^* \approx 2$, or the value of w^* corresponding to $w^* \approx 2 w_c$.

Fig. 7 shows data obtained by several investigators and analyzed by Benkoski, Fredrickson and Kramer [22] for several asymmetric interface pairs. Here, G/G^* is plotted versus the normalized interface width $w = d/d_t$, where d_t is the reptation tube diameter, calculated as $d_t = b(4/5 N_e)^{1/2}$. Significantly, no strength develops below some critical value w_c . The magnitude

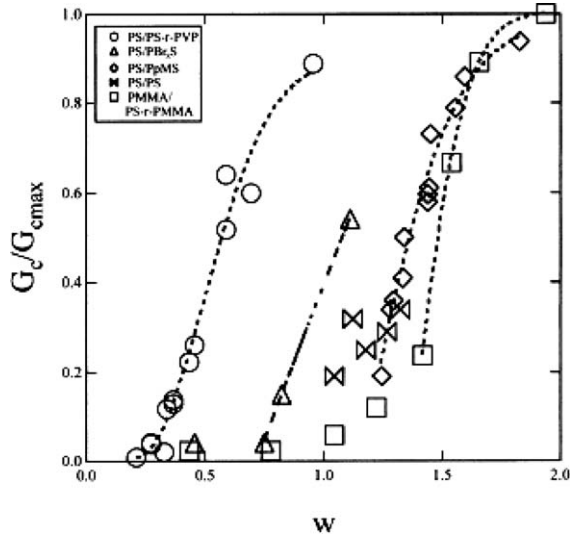


Fig. 7. Data compiled by Benkoski et al. [22] showing the interfacial fracture energy vs. normalized interfacial width w , for several A/B pairs. Circles represent PS/PS-rPVP, boxes PMMA/PS-r-PMMA, diamonds PS/PpMS, triangles PS/PBxS and bowties PS/PS data.

of w_c is of order unity, but varies for each polymer pair due to the slight differences in their normalization procedure ($w = d/d_i$) compared to the above analysis ($w = d/d_c$). However, the slopes are of order unity, as predicted herein, and the maximum strength occurs at $w^* \approx 2$, when $w_c \approx 1$, or at $w^* = 2w_c$. The data in Fig. 7 could be readily normalized to $w_c = 1$ to form a master curve consistent with the very simple relation:

$$G/G^* = w - 1 \quad (5.9)$$

with slope of unity, intercept $w = 1$ and $w^* = 2$. This analysis differs from that provided by Benkoski et al. [22], who developed an interface strength theory based on the added contributions of monomer friction effects and an entanglement segment length distribution. Coupled with the Brown theory of fracture [25,26], this approach produced a more complex expression for G , which gave reasonable agreement with their data in Fig. 7. While being significantly different in their derivation, a major fundamental difference between the theories is that the Benkoski theory requires both friction and entanglements to explain all the data in Fig. 7, while the percolation theory requires only the entanglement effects to explain all the data, since the friction terms are effectively zero on the G/G^* scale.

When $w < w_c$, or $p < p_c$, the Nail solution, $G \sim \Sigma L^2$, applies as the Σ non-entangled chain segments of length L pullout in simple friction. However, the chain segments do not pullout as linear strings of length L , as can be deduced in Fig. 6, but rather as intermeshed random walks of length $L^{1/2}$; the chain segment is attached to a very long chain, which is itself entangled, and hence, will not allow the segment L to pullout as a string. Thus, the critical stress behaves as $\sigma \sim \Sigma \mu L^{1/2}$, where μ is the friction coefficient. The critical crack opening displacement behaves as $\delta \sim L^{1/2}$, such that the fracture energy for pullout is:

$$G \sim \mu \Sigma L \quad (5.10)$$

Since Σ is constant and $L \sim d^2$, it follows that in simple pullout at $w < w_c$:

$$G \sim d^2 \quad (5.11)$$

However, this fracture energy is very low and orders of magnitude lower than that obtained at $w > w_c$. Both theories based on the friction contribution agree with the quadratic dependence $G \sim d^2$, as first proposed by Willett and Wool [21].

The adhesion between immiscible polymers as a function of interfacial width was also analyzed by Cole, Cook and Macosko [23] in terms of the number of entanglements N_{ent} in the interface. They define N_{ent} in the incompatible interface of width d as:

$$N_{\text{ent}} = d/L_c \quad (5.12)$$

where L_c is the entanglement length, defined by $L_c = b [M_e/6 M_0]^{1/2}$, in which M_0 is the monomer molecular weight and b is the bond length. They propose that the resistance to fracture is determined by:

$$G \sim N_{\text{ent}}^2 \quad (5.13)$$

Their data is shown in Fig. 8 (Fig. 7 in Cole et al. [23]), where the slope of 2 from a plot of $\log G$ vs. $\log N_{\text{ent}}$ suggests support for the quadratic dependence in Eq. 5.13. The circles in Fig. 8 represent data obtained from interface pairs consisting of the following; PP/aPA, PS/aPA, PS/PP, PS/PEO, PS/PC, PS/PVC, PS/PE, PS/PMMA, PET/PC, using both melt and solvent lamination. The triangles in Fig. 8 represent literature values for PS-r-PMMA by Brown et al. [25], and the squares represent PC/SAN data obtained by Janarthan

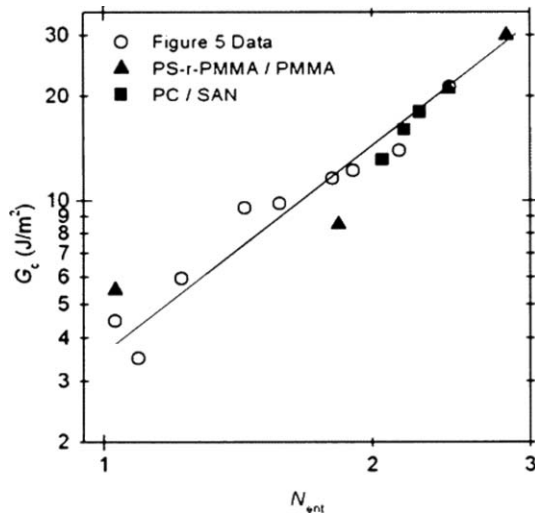


Fig. 8. Fracture energy of A/B incompatible interfaces vs. N_{ent} , as compiled by Cole et al. [23]. The power-law agreement with a slope of 2 (solid line) suggests a relationship of the form $G_c \sim N_{\text{ent}}^2$ adequately describes the adhesion

et al. [87]. Alternatively, using the percolation model, since $p \sim d/L_c$, then from Eqs. (5.5) and (5.12), we obtain:

$$G \sim [N_{\text{ent}} - N_c] \quad (5.14)$$

where N_c is the critical number of entanglements, corresponding to p_c . Normalizing this relation by the maximum strength G^* at N^* , $G^* \sim [N^* - N_c]$, we obtain

$$G/G^* = [N_{\text{ent}} - N_c]/[N^* - N_c] \quad (5.16)$$

Accordingly, a plot of G vs. N_{ent} should give a linear plot with intercept N_c as shown in Fig. 9, using data from Cole et al., (Table 3 in ref [23]). The linear fit correlation coefficient was $R^2 = 0.95$ (neglecting

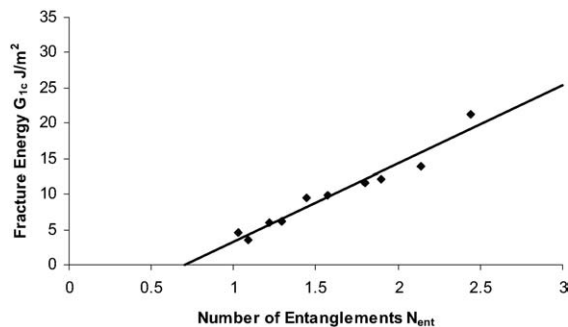


Fig. 9. A plot of fracture energy vs. N_{ent} , using data of Cole et al. [23] from Fig. 11. The line is a best fit of the data to the percolation relation, $G_{1c} \sim [N_{\text{ent}} - N_c]$.

$G = 0$ points) with intercept $N_c = 0.7$, and slope of 11 J/m^2 . Cole et al. observed at least three $G = 0$ values in the vicinity of N_c , supporting the concept that little, or no strength exists below the percolation threshold

Thus, the data in Fig. 9 is linear with a non-zero intercept as expected, which meaningfully divides the data into two regions, $N_{\text{ent}} < N_c$ for which $G \approx 0$, consistent with very weak interfaces, and $N_{\text{ent}} > N_c$, which describes the strong interfaces. However, a power law fit with zero intercept, as required by the homogeneous function $G \sim N_{\text{ent}}^\beta$, will suggest an exponent of $\beta \approx 2$, and also describes both weak and strong regions with the same function. Clearly, a plot of $\log G$ vs. $\log [N_{\text{ent}} - N_c]$ would give an exponent of $\beta \approx 1$, consistent with the percolation theory. During welding, N_{ent} behaves as $N_{\text{ent}} \sim t^{3/4} M^{-7/4}$ (Table 1), which we observe experimentally [1]. However, if one were to use the strength relation $G_{1c} \sim N_{\text{ent}}^2$, one would predict that $G_{1c} \sim t^{3/2} M^{-7/2}$, and $G^* \sim M^{-2}$, which is universally inconsistent with all welding and virgin-state data.

6. Fracture of reinforced incompatible interfaces

The role of A–B diblock compatibilizers or random A–B copolymers of aerial density Σ at incompatible A/B interfaces was investigated by Creton, Brown, Char, Deline and Kramer et al. [24–31]. Fig. 10 shows results of G_{1c} vs. Σ for PS/PMMA interfaces reinforced by PS(800)–PVP(870) diblocks. Most of the data are reasonably well described by a line with a slope of 2 on this log–log plot, suggestive of $G \sim \Sigma^2$. Brown analyzed this and other similar data and derived a theory of fracture, which is referred as the Σ^2 law [25,26]:

$$G_{1c} \sim \Sigma^2 / \sigma_{\text{cr}} \quad (6.1)$$

in which σ_{cr} is the yield stress in the craze zone at the crack tip. If the $G_{1c} \sim \Sigma^2$ law is applied to welding, from Table 1 $\Sigma(t) \sim t^{1/4} M^{-5/4}$ and $\Sigma_\infty \sim M^{-1/2}$, then one obtains $G_{1c} \sim t^{1/2} M^{-5/2}$ and $G^* \sim 1/M^2$, when $\tau^* \sim M$. Despite the correct time dependence ($t^{1/2}$) of welding, the predictions are not in accord with both the molecular weight dependence of welding, and particularly that of the virgin state, where contrary to all data, it is predicted that the strength decreases with increasing molecular weight. Alternatively, using Eq. (6.1), we can let $\sigma_{\text{cr}} \sim X$, such that $G_{1c} \sim t^{1/4} M^{-9/4}$. While the $t^{1/4}$ dependence is not observed in the usual

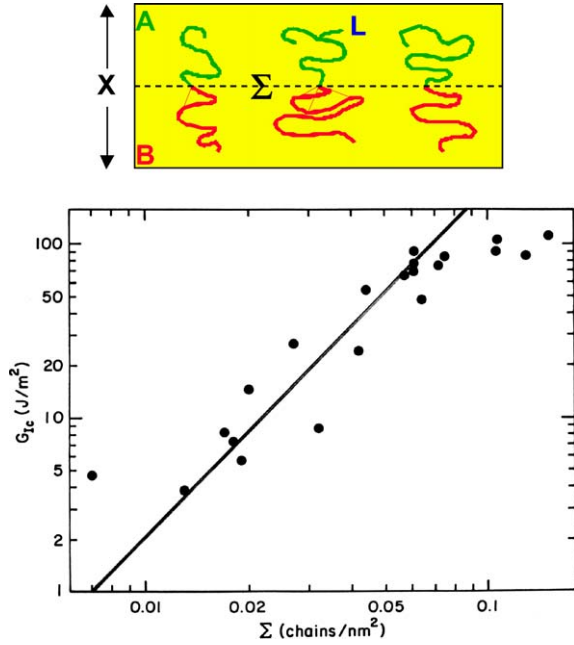


Fig. 10. Fracture energy G_{1c} vs. areal chain density Σ , data reported by Creton et al. [27] for the PS(800)-PVP(870) diblock reinforced PS/PMMA incompatible interface. The solid line was drawn with a slope of 2, suggestive of the scaling law $G_{1c} \sim \Sigma^2$.

case, it could occur if the chain ends were segregated to the weld surfaces, but this was not observed to occur experimentally in the HDH/DHD experiments of Welp et al. [73–78] and essentially all welding data supports the $t^{1/2}$ dependence. So, the Brown model is incompatible with the Wool welding model, and visa versa. We can reconcile these differences within the framework of the percolation model, which predicts that $G \sim [p - p_c]$, as:

$$G_{1c} \sim [(\Sigma L/X) - (\Sigma L/X)_c] \quad (6.2)$$

Since L and X are constant, then $p_c \sim \Sigma_c$, which represents a critical number of chains required to build up the network above the percolation level. Letting $L/X \sim R_{gA}$ of the diblock ends, the percolation model predicts the linear relation:

$$G_{1c} \sim R_{gA} [N - N_c] \quad (6.3)$$

Normalizing this relation by the maximum strength G^* at Σ^* , we have:

$$G/G^* = [\Sigma - \Sigma_c]/[\Sigma^* - \Sigma_c] \quad (6.4)$$

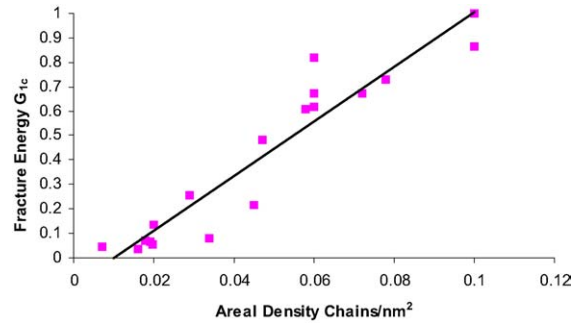


Fig. 11. Fracture energy (normalized) G/G^* vs. areal density Σ , of A–B diblock chains in an A/B incompatible interface, using data of Creton et al. [27] from Fig. 10. The line is a least-square fit to the percolation formula, $G/G^* \sim [\Sigma - \Sigma_c]$.

Fig. 11 shows a plot of G/G^* vs. Σ , using Creton’s data from Fig. 10. The fracture data was normalized by $G^* \approx 110 \text{ J/m}^2$, which is the upper range of the data presented in Fig. 10. The linear relation for G/G^* vs. Σ had a correlation coefficient of 0.9 and produced an intercept on the Σ -axis of $\Sigma_c = 0.1/\text{nm}^2$. The slope of this line is $11.1/\text{nm}^2$. The transition from Nails to Nets, or weak to strong interfaces, is demarcated by the threshold value Σ_c , which, as discussed by Creton et al., should occur near the overlap of the diblock random coils in the interface, such that:

$$\Sigma_c \approx 1/R_{gA}^2 \quad (6.5)$$

The radius of gyration of the PS ends with $M_n = 83\,200 \text{ g/mol}$ is $R_{gA}^2 = 63.2 \text{ nm}^2$, such that $\Sigma_c \approx 0.016 \text{ nm}^2$, which is in reasonable accord with the experimental value $\Sigma_c = 0.01/\text{nm}^2$ in Fig. 11. The maximum value of Σ^* at G^* can be determined from the entanglement bridge theory [66] by:

$$\Sigma^* = [M_c/M^*]^{1/2}/2a \quad (6.6)$$

where $a \approx 1 \text{ nm}^2$ is the cross-sectional area of a bridge segment of a diblock chain as it crosses the interface. For polystyrene, with $M_c = 30,000$ and a molecular weight of $M^* = 250\,000 \text{ g/mol}$, then $\Sigma^* \approx 0.17 \text{ nm}^2$. When brush-like ordering occurs at the interface, $L \approx 0$ as M_c increases, and G_{1c} decreases considerably.

Examining both theories, $G_{1c} \sim \Sigma^2$ and $G_{1c} \sim [\Sigma - \Sigma_c]$, as plotted in Figs. 10 and 11, respectively, there is sufficient data scatter in both plots such that one could not judge, based on this data alone, as to which theory was more valid. However, the percolation model, in addition to describing the A/B reinforced interface above,

is universally consistent with welding data, virgin-state strength and the transition from weak to strong interfaces. It can be deduced that the exponent of 2, reported in several instances, is an accidental consequence of inhomogeneous functions for G_{1c} vs. N_{ent} with incompatible A/B interfaces, G_{1c} vs. Σ data for reinforced A/B interfaces and G_{1c} vs. M for virgin strength data. The percolation theory of incompatible interfaces is significantly different and in contradiction with theories proposed by Benkoski et al., Cole et al. and Brown et al.

7. Conclusion

A theory of fracture of entangled polymers was developed which was based on the vector percolation model of Kantor and Webman, in which the modulus E

is related to the lattice bond fraction p , via $E \sim [p - p_c]^5$. The polymer fractured critically when p approached the percolation threshold p_c , which was accomplished by utilizing the stored strain energy in the network to randomly fracture $[p - p_c]$ bonds. The fracture energy was found to be $G_{1c} \sim [p - p_c]$. When applied to interfaces of width X , containing an areal density Σ of chains, each contributing L entanglements, the percolation term $p \sim \Sigma L/X$, and the percolation threshold was related to Σ_c , L_c , or X_c . This gave a unified theory of fracture for the virgin state of polymers in the bulk and a variety of polymer interfaces. The percolation theory has also been applied successfully to fracture of carbon nanotubes [3,88,89] and polymer–solid interfaces [90–92].

Several important results are summarized in Table 2 and include the following:

(1) the fracture strength σ of amorphous and semicrystalline polymers in the bulk could be well described

Table 2
Interface and bulk properties

| Polymer system | Property | Relation | Comment |
|----------------------------------|---|---|--|
| Symmetric A/A | Welding fracture energy G_{1c} | $G_{1c} = G^* (t/\tau)^{1/2}$ | $\tau \sim M$, $M > M^*$ $\tau \sim M^3$, $M < M^*$ $M^* = 8 M_c$ $\tau^* = 64 (M_c/M)^2 T_r$ |
| A/A | Toughness K_{1c} | $K_{1c} \sim t^{1/4} M^{-1/4}$ | $G_{1c} = K_{1c}^2/E$ |
| A/A | Welding below T_g | $G_{1c} \sim \Delta T^{-2\nu}$ $X_c = b(1 - p_c) / \{p_c^\nu [1 - TT_g]^\nu\}$ | $\nu = 0.82$ $b = 0.154 \text{ nm}$ $p_c = 0.4$ |
| A/A | Chain-end segregation | $G_{1c} = G^* (t/\tau)^{1/4}$ | $p \sim X$ |
| A Thin film | T_g vs h | $T_g(h) = T_g^\infty [1 - (B/h)^\gamma]$ | $\gamma = 1/[\nu(D - d + 1)]$ $B = S b/p^*$ |
| Virgin state | Fracture energy G_{1c} | $G_{1c}/G^* = 0.3 M/M_c [1 - (M_c/M)^{1/2}]^2$ | Disentanglement $M < M^*$ $M_c = M_e/(1 - p_c)$ |
| Virgin state | G_{1c} | $G_{1c} = G^* [1 - M_c/M]$ | Bond rupture $M > M^*$ |
| Virgin state | G_{1c} | $G_{1c} = G_o + k M$ | $M < M_c$ $G_o = 2 \gamma S$ |
| Fatigue | da/dN | $da/dN \sim X^{-5}$ | $T_r \sim M^3$ necessary |
| Net solution | Fracture stress σ | $\sigma^* = \{2 E \nu D_o [p - p_c]\}^{1/2}$ | $D_o = \text{C-C bond energy}$ |
| A/B Incompatible interface | Fracture energy G | $G \sim [d - d_c]$ $G/G^* = (w - 1)/(w^* - 1)$ $G \sim [N_{ent} - N_c]$ | $w = d/d_c$ $d = 6 b/\chi^{1/2}$ $N_{ent} = d/L_c$ |
| Incompatible with Σ (A-B) | Fracture energy G | $G_{1c} \sim R_{gA} [N - N_c]$ | $\Sigma_c \approx 1/R_{gA}^2$ |
| Rubber | Fracture stress σ and energy G | $\sigma \sim \nu$ $\sigma \sim E$ $G \sim \nu$ | $E \sim \nu k T$ $\nu \sim 1/M_x$ |
| Thermosets | Fracture stress σ , energy G | $\sigma \sim [E \nu]^{1/2}$ $G \sim \nu^{-1/2}$ | $\nu = \text{crosslink density}$ |

The factor of 8 rather than 16 occurs due to an orientation correction [1].² R. P. Wool, American Physical Society Meeting (2000).

by the net solution, $\sigma = [ED_o\rho/16M_c]^{1/2}$, and found to be in excellent agreement with a large body of data. This is a first-principles approach to fracture and requires no fitting parameters;

- (2) for welding of A/A symmetric interfaces, $p = \Sigma L/X$, and $p_c \approx L_c/M \approx 0$, such that when $\Sigma/X \sim 1/M$ for randomly distributed chain ends, $G/G^* = (t/\tau^*)^{1/2}$, where $\tau^* \sim M$, when $M > M^*$, and $\tau \sim M^3$, when $M < M^*$. When the chain ends are segregated to the surface, Σ is constant with time and $G/G^* = [t/\tau^*]^{1/4}$;
- (3) for incompatible A/B interfaces of width d , normalized width w , and entanglement density $N_{ent} \sim d/L_c$, $p \sim d$ such that $G \sim [d - d_c]$, $G \sim [w - 1]$, and $G \sim [N_{ent} - N_c]$;
- (4) for incompatible A/B interfaces reinforced by an areal density Σ of compatibilizer chains, L and X are constant, $p \sim \Sigma$, $p_c \sim \Sigma_c$, such that $G \sim [\Sigma - \Sigma_c]$.

Acknowledgments

The author is grateful to the National Science Foundation and the Environmental Protection Agency for financial support of this work.

References

- [1] R.P. Wool, *Polymer Interfaces: Structure and Strength*, Hanser Press, New York, 1995.
- [2] R.P. Wool, Chapter 8, in: M. Chaudhury, A.V. Pocius (Eds.), *Adhesion Science and Engineering*, Vol. 2, Elsevier, New York, 2002.
- [3] R.P. Wool, *J. Polym. Sci. Part B: Polym. Phys.* 43 (2005) 168.
- [4] S.S. Voyutskii, *Autohesion and Adhesion of High Polymers*, John Wiley & Sons, New York, 1963.
- [5] H.H. Kausch, K. Jud, *Plastics Rubber Proc. Appl.* 2 (1982) 265.
- [6] H.H. Kausch, *Pure Appl. Chem.* 55 (1983) 833.
- [7] K. Jud, J.G. Williams, H.H. Kausch, *J. Mater. Sci.* 16 (1982) 204.
- [8] S. Prager, M. Tirrell, *J. Chem. Phys.* 75 (1981) 5194.
- [9] P.-G. de Gennes, *C.R. Acad. Sci. Paris, Ser. II* 307 (1988) 1841.
- [10] P.-G. de Gennes *C. R. Acad. Sci. Paris, Ser. B* 291 (6) (1980) 219; *C. R. Acad. Sci., Paris, Ser II* 292 (1981) 1505.
- [11] P.-G. de Gennes, L. Léger, *Annu. Rev. Phys. Chem.* 33 (1982) 49.
- [12] P.-G. de Gennes, *Europhys. Lett.* 15 (2) (1991) 191.
- [13] P.-G. de Gennes, *J. Phys. Fr.* 50 (1989) 2551.
- [14] P.-G. de Gennes, *C.R. Acad. Sci. Paris, Ser. II* 308 (1989) 13.
- [15] E. Raphael, P.-G. de Gennes, *J. Chem. Phys.* 96 (1992) 4002.
- [16] R.P. Wool, K.M. O'Connor, *J. Appl. Phys.* 52 (1981) 5953.
- [17] R.P. Wool, K.M. O'Connor, *J. Polym. Sci.: Polym. Lett. Ed.* 20 (1982) 7.
- [18] R.P. Wool, B.-L. Yuan, O.J. McGarel, *Polym. Eng. Sci.* 29 (1989) 1340.
- [19] Y.H. Kim, R.P. Wool, *Macromolecules* 16 (1983) 11.
- [20] H. Zhang, R.P. Wool, *Macromolecules* 22 (1989) 3018.
- [21] J.L. Willett, R.P. Wool, *Macromolecules* 26 (1993) 5336.
- [22] J.J. Benkoski, G.H. Fredrickson, E.J. Kramer, *J. Polym. Sci., Part B: Polym. Phys.* 40 (2002) 2377.
- [23] P.J. Cole, R.F. Cook, C.W. Macosko, *Macromolecules* 36 (2003) 2808.
- [24] C. Creton, E.J. Kramer, H.R. Brown, C.Y. Hui, *Adv. Polym. Sci.* 156 (2002) 53.
- [25] H.R. Brown, *Macromolecules* 24 (1991) 2752; 34 (2001) 3720.
- [26] H.R. Brown, *J. Mater. Sci.* 25 (1990) 2791.
- [27] C. Creton, E.J. Kramer, C.-Y. Hui, H.R. Brown, *Macromolecules* 25 (1992) 3075.
- [28] C. Creton, E.J. Kramer, *Macromolecules* 24 (1991) 1846.
- [29] K. Cho, H.R. Brown, D.C. Miller, *J. Polym. Sci., Part. B: Polym. Phys.* 28 (1990) 1699.
- [30] H.R. Brown, K. Char, V.R. Deline, P.F. Green, *Macromolecules* 26 (1993) 4155.
- [31] K. Char, H.R. Brown, V.R. Deline, *Macromolecules* 26 (1993) 4164.
- [32] K.L. Anderson, J.T. Wescott, T.J. Carver, A.H. Windle, *Mater. Sci. Eng. A* 365 (1–2) (2004) 14.
- [33] J. Rottler, M.O. Robbins, *J. Adhes. Sci. Technol.* 17 (3) (2003) 369.
- [34] R.P. Wool, J.M. Long, *Macromolecules* 26 (1993) 5227.
- [35] E. Helfand, *Macromolecules* 25 (1992) 1676.
- [36] V. Ganesan, V. Pryamitsyn, *Macromolecules* 35 (2002) 9219.
- [37] R.E. Gorga, B. Narasimhan, *J. Polym. Sci., Part B: Polym. Phys.* 20 (2002) 2292.
- [38] A.G. Mikos, N.A. Pappas, *J. Chem. Phys.* 88 (1988) 1337.
- [39] M. McLeish, M. Plummer, A. Donald, *Polymer* 30 (1989) 1651.
- [40] R.P. Wool, D. Bailey, A. Friend, *J. Adhes. Sci. Technol.* 10 (1996) 305.
- [41] H.P. Schreiber, A. Ouhlal, *J. Adhes.* 79 (2) (2003) 141.
- [42] R. Schnell, M. Stamm, C. Creton, *Macromolecules* 32 (1999) 3240.
- [43] Y.C. Wang, M.A. Winnik, *Macromolecules* 26 (12) (1993) 3147.
- [44] J.N. Yoo, L.H. Sperling, C.J. Glinka, A. Klein, *Macromolecules* 23 (1990) 3962.
- [45] N. Mohammadi, A. Klein, L.H. Sperling, *Macromolecules* 26 (1993) 1019.
- [46] M. Sambasivan, A. Klein, L.H. Sperling, *J. Appl. Polym. Sci.* 58 (2) (1995).
- [47] D.B. Kline, R.P. Wool, *Polym. Eng. Sci.* 28 (1988) 52.
- [48] R.E. Robertson, *Toughness and Brittleness of Plastics*, Adv. Chem. Ser. 154, Am. Chem. Soc., Washington, DC, 1976.

- [49] E.J. Kramer, *J. Mater. Sci.* 14 (1978) 1381.
- [50] F. Yang, R. Pitchumani, *Macromolecules* 35 (2002) 3213.
- [51] Y.M. Boiko, *Mech. Composite Mater.* 31 (1) (2003) 89.
- [52] Y.M. Boiko, A. Bach, J. Lynaae-Jorgensen, *J. Polym. Sci., Part B: Polym. Phys.* 42 (2004) 1861.
- [53] J.W. Hutchinson, Liking Scales in Fracture mechanics Plenary Address, Proc. Ninth International Conference on Fracture, Sydney, Australia, April 1997.
- [54] V. Tvergaard, J.W. Hutchinson, *J. Mech. Phys.: Solids* 41 (6) (1993) 1119.
- [55] V. Tvergaard, J.W. Hutchinson, *J. Phys. IV* 6 (C6) (1996) 165.
- [56] Y. Kantor, I. Webman, *Phys. Rev. Lett.* 52 (1984) 1891.
- [57] S. Feng, B.I. Halperin, P.N. Sen, *Phys. Rev. B* 35 (9) (1987) 197.
- [58] S. Feng, M.F. Thorpe, E. Garboczi, *Phys. Rev. B* 31 (1) (1985) 276.
- [59] H. He, M.F. Thorpe, *Phys. Rev. Lett.* 54 (19) (1985) 2107.
- [60] E.J. Garboczi, M.F. Thorpe, *Phys. Rev. B* 31 (11) (1985) 7276.
- [61] M.F. Thorpe, E.J. Garboczi, *Phys. Rev. B* 35 (16) (1987) 8579.
- [62] P.-G. de Gennes, *J. Phys. Lett. (Paris)* 37 (1976) L1.
- [63] M. Born, K. Huang, *Dynamical Theory of Crystal Lattices*, Oxford University Press, New York, 1954.
- [64] R.P. Wool, R.S. Bretzlaff, B.Y. Li, C.H. Wang, R.H. Boyd, *J. Polym. Sci., Part B: Polym. Phys.* 24 (1986) 1039.
- [65] R.P. Wool, *Polym. Eng. Sci.* 20 (1980) 805.
- [66] R.P. Wool, *Macromolecules* 26 (1993) 1564.
- [67] A. Uhlherr, M. Doxastakis, V.G. Mavrantzas, D.N. Theodorou, S.J. Leak, N.E. Adam, P.E. Nyberg, *Europhys. Lett.* 57 (4) (2002) 506.
- [68] D.N. Theodorou, *Mol. Phys.* 102 (2) (2004) 147.
- [69] A.M. Donald, E.J. Kramer, *J. Mater. Sci.* 16 (1981) 2977.
- [70] P.J. Flory, *Principles of Polymer Chemistry*, Cornell University Press, Ithaca, NY, 1953.
- [71] T.P. Lodge, *Phys. Rev. Lett.* 83 (1999) 3218.
- [72] M. Doi, S.F. Edwards, *The Theory of Polymer Dynamics*, Clarendon Press, Oxford, UK, 1986.
- [73] K.A. Welp, R.P. Wool, J. Mays, A. Pispas, S. Satija, *Macromolecules* 31 (15) (1998) 49.
- [74] G. Agrawal, R.P. Wool, W.D. Dozier, G.Z.P. Felcher, J. Zhou, J.W. Mays, T.P. Russell, *J. Polym. Sci., Part B: Polym. Phys.* 34 (1996) 2919.
- [75] T.P. Russell, V.R. Deline, W.D. Dozier, G.P. Felcher, G. Agrawal, R.P. Wool, J.W. Mays, *Nature* 365 (1993) 235.
- [76] G. Agrawal, R.P. Wool, W.D. Dozier, G.P. Felcher, T.P. Russell, J.W. Mays, *Macromolecules* 27 (1994) 4407.
- [77] S.J. Whitlow, R.P. Wool, *Macromolecules* 22 (1989) 2648; 24 (1991) 5926.
- [78] K.A. Welp, R.P. Wool, G. Agrawal, S.K. Satija, S. Pispas, J. Mays, *Macromolecules* 32 (15) (1999) 5127.
- [79] R.P. Wool, *Rigidity Percolation Theory of Thin Films and the Glass Transition*, PMSE Preprints, Am. Chem. Soc., Philadelphia, August 2004.
- [80] B. Sapoval, M. Rosso, J.F.J. Gouyet, *Phys. Lett.* 46 (1985) L149.
- [81] P.-G. de Gennes, *J. Chem. Phys.* 55 (1971) 572.
- [82] S.F. Edwards, *J. Chem. Soc., Lond.* 92 (1967) 9.
- [83] J.-P. Cohen Addad, A. Guillermo, *Macromolecules* 36 (2003) 1609.
- [84] P. Green, E.J. Kramer, *J. Mater. Res.* 1 (1) (1986) 202.
- [85] V. Janarthanan, R.S. Stein, P.D. Garrett, *Macromolecules* 27 (1994) 4855.
- [86] O.K.C. Tsui, H.F. Zhang, *Macromolecules* 34 (2001) 9139.
- [87] J.A. Keddie, R.A.L. Jones, R.A. Cory, *Faraday Discuss.* 98 (1994) 219.
- [88] R.P. Wool, *Bio-Based Composites*, Proc. European Congress on Composite Materials (ECCM-11), Rhodes, Greece, 2 June 2004.
- [89] R.P. Wool, X.S. Sun, *Bio-Based Polymers and Composites*, Elsevier, Burlington MA, USA, 2005.
- [90] I. Lee, R.P. Wool, *J. Polym. Sci., Part B: Polym. Phys.* 40 (20) (2001) 2343.
- [91] I. Lee, R.P. Wool, *J. Adhes.* 75 (2001) 299.
- [92] L. Gong, R.P. Wool, *J. Adhes.* 71 (189) (1999).